A CFD Analysis of Compressible Flow Through Convergent-Conical Nozzles

Nathan Spotts*, Stephen Guzik †and Xinfeng Gao‡
CFD and Propulsion Laboratory
Colorado State University, Fort Collins, Colorado, USA

Work presented at the 1st Propulsion Aerodynamics Workshop on the CFD study of compressible flow through convergent-conical nozzles is summarized. This work focused on assessing the accuracy of the CFD study in obtaining nozzle performance and flow structure, including nozzle thrust and discharge coefficients and the shock structure. The CFD studies were performed using Metacomp CFD++ software and compared with the available experimental data during the workshop. We confirmed that the discharge coefficient increases as the nozzle angle decreases and the choked nozzle pressure ratio is lower for a smaller nozzle angle. The discharge coefficient increases with increasing pressure ratio until the choked condition is reached. The thrust coefficient increases as the nozzle angle increases, and for a given nozzle angle, the thrust coefficient decreases as nozzle pressure ratio increases. Results and assessments are presented in this paper and at the 49^{th} AIAA Joint Propulsion Conference.

Nomenclature

α	nozzle angle
amb	ambient conditions
A	area
C_d	discharge coefficient
C_t	thrust coefficient
γ	ratio of specific heats
$\dot{m}$	mass flow rate
NPR	nozzle pressure ratio
o	quantity at the nozzle inlet
Ψ	flow factor
p	static pressure
P	stagnation pressure
ρ	density
$\mathcal{R}$	specific gas constant
R	nozzle throat radius
T	stagnation temperature
u	local axial velocity
U	average axial velocity
$*$	critical conditions
$ideal$	quantity calculated based on one-dimensional isentropic flow assumption

*Masters Student, Department of Mechanical Engineering, email: nspotts@engr.colostate.edu, Student Member.
†Research Scientist, Department of Mechanical Engineering, email: Stephen.Guzik@colostate.edu, AIAA Member.
‡Assistant Professor, Department of Mechanical Engineering, email: Xinfeng.Gao@colostate.edu, AIAA Member.

I. Introduction

The Propulsion Aerodynamics Workshop (PAW) promotes a benchmark for assessing the accuracy of current CFD technology in obtaining multi-stream air breathing jet performance and flow structure.The PAW also provides a forum for discussion among the community of engineers and scientists interested in the analysis and assessment of the aerodynamics of installed propulsion systems. We participated in the first PAW and presented a CFD study of compressible flow through convergent-conical nozzles. The convergent-conical nozzle type was of interest to this study because the exhaust nozzle of the jet propulsion system is often of convergent-conical type. Moreover, Thornock and Brown[1] performed an experimental study of compressible flow through this type of nozzle, including a comparison with the theoretical analysis, in order to evaluate the effect of nozzle shape on the performance of convergent-conical nozzles. By varying the nozzle angle, they examined the nozzle shape effect on performance. In addition, the effect of nozzle pressure ratio was investigated and the value of the choked pressure ratio was determined. Therefore, PAW selected the nozzle geometry and experimental data of Thornock and Brown[1] as the primary reference for the nozzle CFD study.

We performed a CFD study using the Metacomp `CFD++` software.[2] Through this study, we evaluated the accuracy of the `CFD++` software and assessed the comparison between computation, experiment, and theory. We provided our final CFD result to the workshop as the organizers are interested in benchmarking the accuracy of current CFD technology in obtaining multi-stream air breathing jet performance and flow structure.

II. Computational Configuration

II.A. Nozzle Geometry and Mesh

Our CFD study was conducted on axisymmetric nozzles of 15°, 25°, and 40° cone-half-angle (See Fig. 1 for the cone-half-angle indicated by α), in addition to an axisymmetric reference nozzle (Fig. 2). The nozzle geometry consists of a convergent truncated cone preceded by an approach section. Unlike the constant diameter approach section described by Thornock and Brown,[1] the approach section of the computational configuration has an inlet diameter of 5.7275 inches and diverges linearly to a diameter of 5.79 inches before the approach section meets the conical section. The diameter of the nozzle exit is 3.0 inches for all nozzles. The difference between the conical nozzles and the reference nozzle is that the latter is a convergent nozzle with a circular-arc wall contour of 5.449 inches radius. In addition, the workshop provided a mesh for the 25° conical nozzle bifurcated by a splitter plate, in order to investigate the effect of the plate on the nozzle flow field. Note that the exit area is the same for all the nozzles. According to the categorization by the PAW, the nozzle cases are grouped into three instances. Instance ① includes four axisymmetric nozzles, i.e., the reference nozzle and three conical nozzles with the cone-half-angles of 15°, 25°, and 40°. The nozzle pressure ratio (NPR) range under investigation is from 1.4 to 7.0, making up eleven cases of 1.4, 1.6, 1.8, 2.0, 2.5, 3.0, 3.5, 4.0, 5.0, 6.0, and 7.0 for each axisymmetric nozzle. Nozzle pressure ratio is defined as the ratio of nozzle total pressure at the nozzle inlet to ambient pressure, P_o/p_{amb}. Instance ② consists of two cases, the 25° conical axisymmetric nozzle and the 25° conical nozzle bifurcated by the splitter plate (Fig. 3). The objective is to compare the jet plumes resulting from them for a NPR of 4.0. Instance ③ is designed to study the time-accurate simulation of vortex shedding due to the splitter plate for a NPR of 1.6. However, the mesh provided by PAW may be too coarse to capture the vortex shedding phenomenon. For this paper, we studied the first two instances.

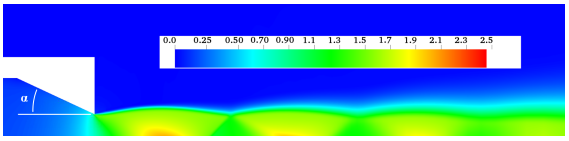

Figure 1. The conical nozzle geometry with α as the cone-half-angle (15°, 25°, 40°).

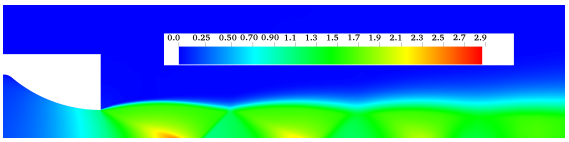

Figure 2. The reference nozzle geometry.

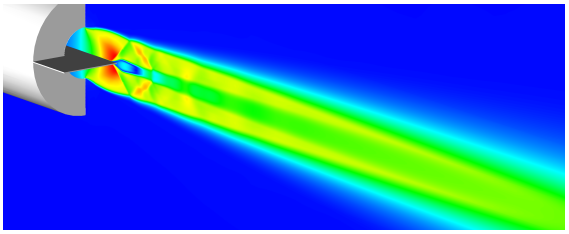

Figure 3. The 25° conical nozzle with the splitter plate.

The AIAA PAW organizers provided overset meshes for all calculations. The meshes for Instance ① are composed of approximately 140,000 hexahedral cells in four component meshes represented by different colors in Fig. 4. These meshes comprise two angular degrees of the axisymmetric domain in the circumferential direction. Two cells are used in the circumferential direction, with degenerated hexahedral cells at the axis of symmetry. The computational domain extends axially from 22.6 inches upstream of the nozzle exit plane to 379.0 inches downstream and its extent in the radial direction is approximately 71.0 inches. Cells adjacent to the solid wall have a y^+ value less than 6. The mesh used for calculations involving the splitter plate configuration is composed of approximately 11×10^6 cells in 7 component meshes. The computational domain is half of the full three-dimensional domain. This mesh assumes symmetry about the plane parallel to the splitter plate and coincident with its center. The extent of this mesh in the axial and radial directions is identical to the axisymmetric mesh used for instance ①, as is the thickness of the cells adjacent to the walls.

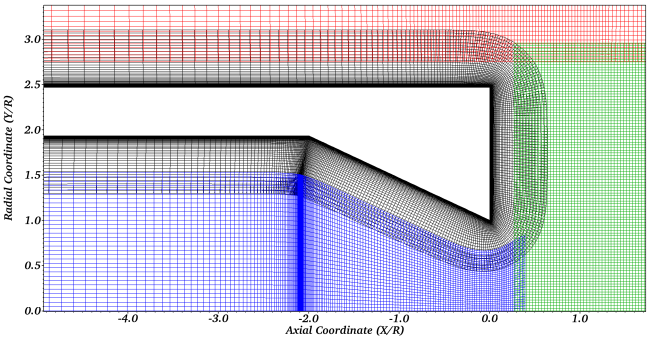

Figure 4. A typical overset mesh created by PAW and used in the simulations.

II.B. Numerical Setups

The working fluid is air and treated as an ideal gas. The nozzles discharge directly into the atmospheric conditions. Boundary conditions are specified for the inlet, outlets, and solid nozzle walls. At the nozzle inlet, total pressure and total temperature are specified. At the outlet, a back pressure is specified. No-slip boundary conditions are applied to the nozzle walls. The thermal wall conditions, both isothermal (atmospheric temperature) and adiabatic, were examined and no significant differences were found in the resultant flow fields.

The CFD solver utilized for this study was `CFD++` from Metacomp Technologies.[2] The compressible, steady-state, Reynolds-averaged, Navier-Stokes equations were solved using a density-based algorithm. The algorithm is based on the finite-volume method with a second-order accuracy in space. A total variation diminishing scheme was employed. A min-mod limiter was adopted for cases of NPR less than 2.0 and a continuous limiter was used for other cases. For nozzle pressure ratios greater than 1.8, minimum dissipation was added by a pressure switch to the right hand side in areas were pressure variations were not smooth. The time integration scheme is implicit and second order accurate. Three turbulence models, the realizable k-ϵ, the Menter shear stress transport, and the realizable q-L model were employed, and they had little impact on both the flow properties of interest and the flow structure near the exit (particularly the location of the sonic line).

III. Simulation Results and Analysis

The nozzle performance is evaluated by the nozzle thrust coefficient, C_t, and the discharge coefficient, C_d. For the 2D axisymmetric nozzle, they are defined by

$$C_t \equiv \frac{\int_0^R [\rho u^2 + (p - p_{\text{amb}})] r dr}{U_{\text{ideal}} \int_0^R \rho u r dr} \qquad \text{and} \qquad C_d \equiv \frac{2\pi \int_0^R \rho u r dr}{\dot{m}_{\text{ideal}}},$$

where ρ, u, and p are local density, axial velocity, and pressure, respectively on the integration path. The radius and area at the nozzle exit are denoted by R and A_{throat}, respectively. The subscript, "ideal", refers to quantities calculated for an ideal nozzle based on one-dimensional isentropic flow assumption. The isentropic mass flow rate, $\dot{m}_{\text{ideal}}$, is calculated by[3]

$$\dot{m}_{\text{ideal}} = \frac{\Psi P_{\text{o}} A_{\text{throat}}}{\sqrt{(\gamma \mathcal{R} T_{\text{o}})}}, \quad \Psi = \begin{cases} \frac{2\gamma^2}{\gamma-1} \frac{p_{\text{throat}}}{P_{\text{o}}} [1 - (\frac{p_{\text{throat}}}{P_{\text{o}}})^{(\gamma-1)/\gamma}] & : p_{\text{throat}} < p^\star \\ \gamma (\frac{2}{\gamma+1})^{(\gamma+1)/(2(\gamma-1))} & : p_{\text{throat}} \geq p^\star \end{cases}, \quad p^\star = (\frac{2}{\gamma+1})^{\gamma/(\gamma-1)},$$

where Ψ is the flow factor, p_{throat} is the static pressure at the nozzle throat, $p^\star$ the critical pressure,[3] γ the specific heat ratio, $\mathcal{R}$ the specific gas constant, and P_o and T_o are specified stagnation conditions at the inlet. The ideal velocity, U_{ideal}, based on an ideal convergent-divergent nozzle operating at the same pressure ratio, is computed by $U_{\text{ideal}} = \sqrt{\frac{2\gamma\mathcal{R}T_\text{o}}{\gamma-1}\left(1-(\frac{p_{\text{throat}}}{P_\text{o}})^{(\gamma-1)/\gamma}\right)}$. Using above relations, we calculated both the nozzle thrust coefficient and the discharge coefficient for all the cases in the instance ①. What follows are the comparisons between the CFD results and the experimental and analytical results published by Thornock and Brown[1]

III.A. Numerical Results

Forty-four simulation cases were solved for instance ①. We determined the effect of the nozzle pressure ratios on the thrust and discharge coefficients, as well as the influence of the nozzle angles. In addition, we evaluated the `CFD++` software performance for nozzle studies. Herein, we illustrate some simulation results using the Mach contours for the 25° nozzle. Results for the complete set of instance ① are analyzed and presented in the next section, and they are compared with the literature data. Figures 5(a)–5(h) show the Mach contour for the 25°-nozzle with NPRs from 1.4 to 7.0. Both the axial and the radial coordinates are normalized by the the radius at the nozzle exit. We clearly observe, from Fig. 5(a)–5(h), that the flow field in the throat of the nozzle is nonuniform and the position of the sonic line becomes independent as NPR increases beyond the choked value. For this case, it does not change significantly for NPR greater than 4.0. The shape of the discharging jet depends on NPR.

The observations are as expected and consistent with those in literature.[1,3] Increasing the NPR (by raising the inlet pressure) results in the propagation of a rarefaction wave from downstream of the nozzle towards the nozzle with a wave speed of the absolute local sonic speed. This causes an increase in the mass flow rate. However, when the pressure ratio is equal to or greater than the choked pressure ratio, the wave or the disturbances from the downstream of the nozzle can no longer be propagated upstream and the mass flow rate stays unchanged.

The jet issues as a cylindrical-like stream, as shown in Fig. 5(a) and 5(b). Under the choked conditions, the jet leaving the nozzle is at the choked pressure, which is higher than the back pressure. The underexpanded flow results in an expansion at the nozzle exit. Boundary conditions of ambient pressure at the top and no penetration at the centerline force an alternating pattern of reflecting compression/shock and expansion fans.

From Fig. 5, one can observe the Mach disk downstream of the nozzle for the cases under supercritical conditions. As NPR increases, the Mach disk moves farther downstream and the radius of the Mach disk increases.[4] The Mach disk is a consequence of satisfying mass flow rate and turning angle constraints that are not achievable with oblique waves. The nozzle angle has little effect on both the location and the radius of the Mach disk, as

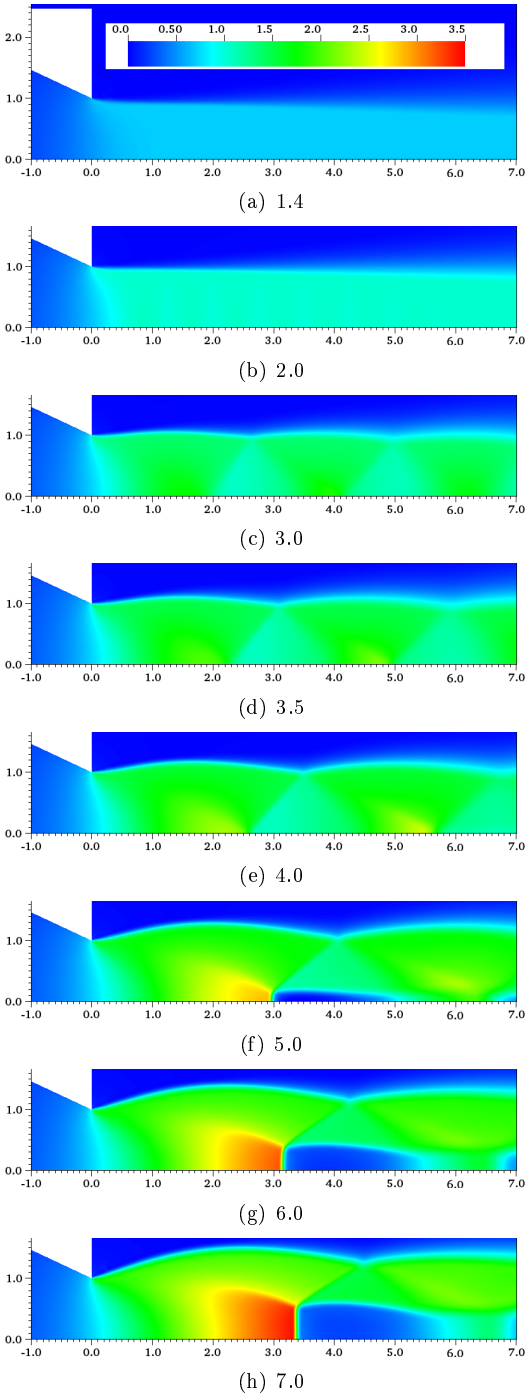

(a) 1.4 (b) 2.0 (c) 3.0 (d) 3.5 (e) 4.0 (f) 5.0 (g) 6.0 (h) 7.0

Figure 5. Mach contours for $\alpha = 40^\text{o}$ with NPR = 1.4–7.0.

shown in Fig. 6 for a NPR of 7.0.

The instance② includes two simulation cases. The diamond shock structure resolved from the CFD result for the 25° axisymmetric nozzle is clearly shown in Fig. 7(a). The contours of the $|\nabla\rho|$ field for the configuration with the splitter plate is displayed on the top half of the Fig. 7(b) in contrast with the bottom half showing the $|\nabla\rho|$ contours for the axisymmetric nozzle.[3] With the splitter plate, the shock location (the intersection between the shock and the axial axis) is moved toward the nozzle and the angle between the shock and the axial axis is smaller. Since the flow is supersonic between the nozzle exit and the shock, features downstream do not influence the flow in this regime. Consequently, the shock location is likely a result of the reduced effective nozzle exit area, perhaps due to boundary layer associated with the splitter plate. Behind the shock, the flow is subsonic and some information can propagate to and affect the shock. The decreased angle is perhaps a result of the plate terminating and small cavity behind it. In summary, the effect of the plate is probably better quantified by the location of the shock rather than the angle.

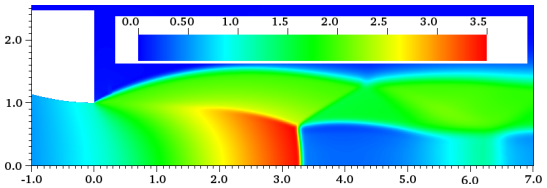

(a) Reference nozzle

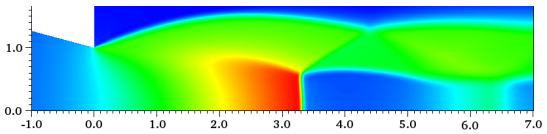

(b) $\alpha = 15^o$

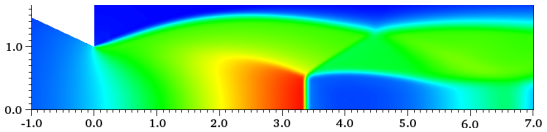

(c) $\alpha = 25^o$

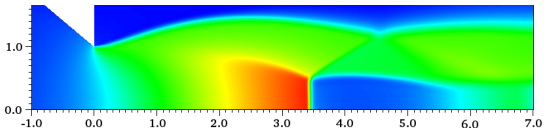

(d) $\alpha = 40^o$

Figure 6. Mach contours for the axisymmetric nozzles at NPR = 7.0.

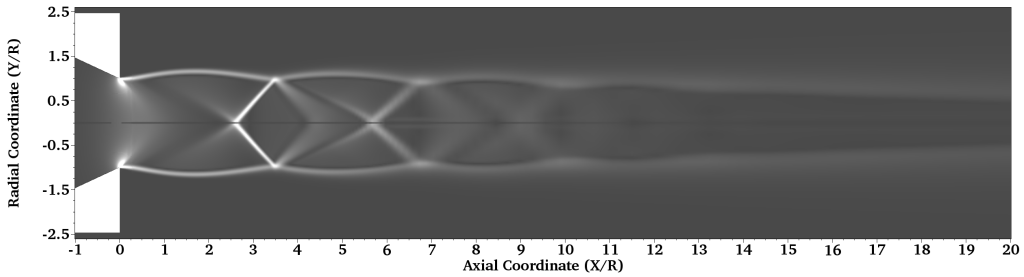

(a) The $|\nabla\rho|$ field for the configuration without the splitter plate showing "diamond" shock structure

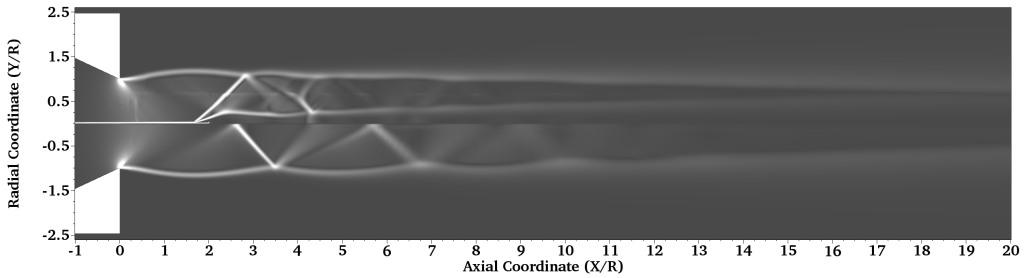

(b) Comparison between the $|\nabla\rho|$ fields, top: with the splitter plate and bottom: without the splitter plate

Figure 7. The comparison between the numerical flow structures for instance②.

III.B. Comparison with Experimental and Analytical Data

We compare the nozzle discharge coefficients and the thrust coefficients predicted from the CFD results to those measured by experiments and the analytical solution. Figure 8(a) shows that, for a given nozzle angle, the discharge coefficient increases with increasing nozzle pressure ratio until the choked condition is reached and, for a given nozzle pressure ratio, the discharge coefficient increases as the nozzle angle decreases. The choked nozzle pressure ratio is smaller for a smaller nozzle angle. Overall, the discharge coefficients based on the CFD result are over-predicted in comparison to both the experimental and analytical data.

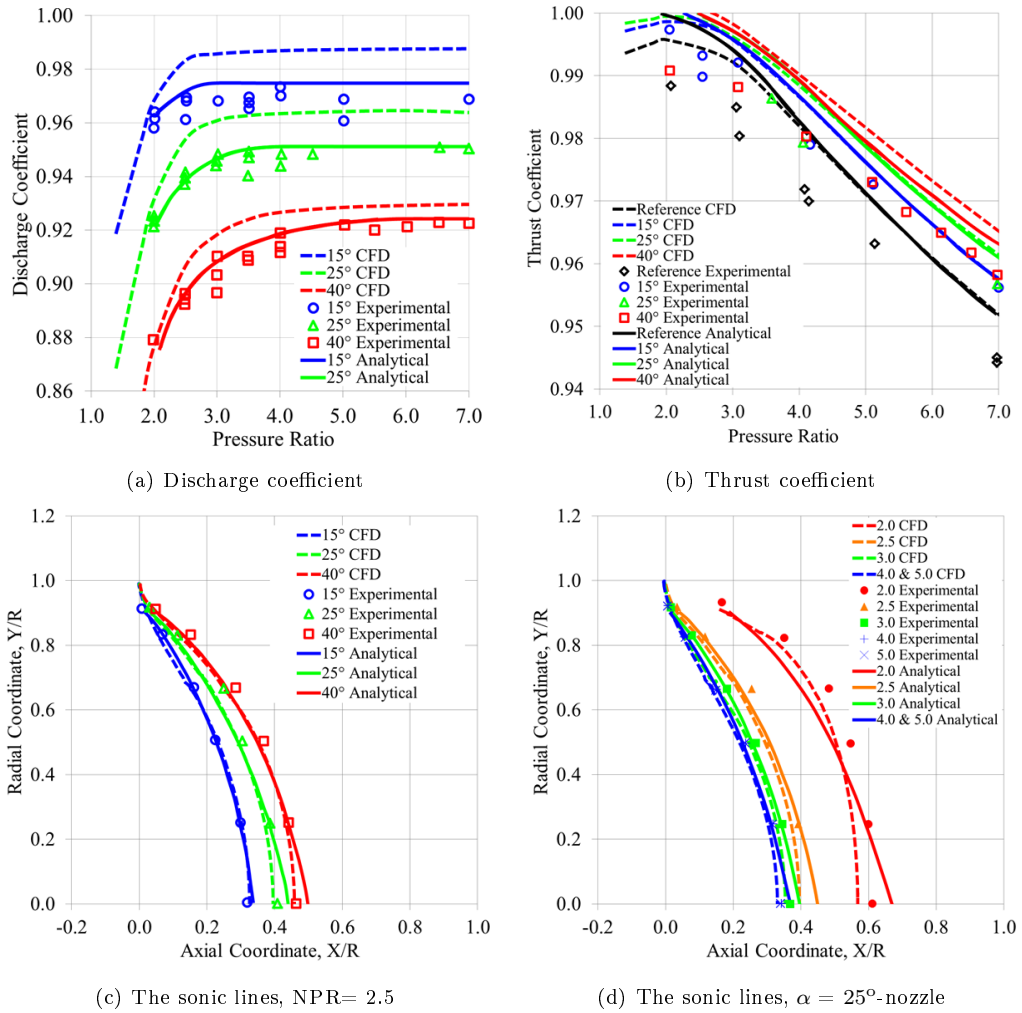

(a) Discharge coefficient

(b) Thrust coefficient

(c) The sonic lines, NPR= 2.5

(d) The sonic lines, α = 25°-nozzle

Figure 8. Comparison of the numerical results to the experimental and analytical data. Subfigure 8(a) compares the discharge coefficients and shows the effect of α and NPR on the discharge coefficients. Subfigure 8(b) compares the thrust coefficients and shows the effect of α and NPR on the thrust coefficients . Subfigure 8(c) compares the sonic lines and shows the effect of α on the location of the sonic lines. Subfigure 8(a) compares the sonic lines and shows the effect of NPR on the location of sonic lines.

We believe that the source for this discrepancy is an imbalance between the predicted inflow and outflow mass. Although the solutions seem to be well converged, as measured by reductions in normalized residuals and stability of both nozzle coefficients and mass flow rates with increasing iterations, the magnitude of the mass flow imbalance is similar to that of the discharge coefficient discrepancy, approximately 1∼2%. Because the nonconservation of mass could result from the mesh, the numerical techniques, or some interaction of the two, further investigation would be required to determine the cause of the imbalance.

Figure 8(b) shows the thrust coefficients computed for the 15°, 25° and 40° nozzles, as well as those for the reference nozzle, in comparison to the experimental data and the analytical solution. The reference nozzle exhibits a lower value of thrust coefficient than those of the conical nozzles. The thrust coefficient increases

as the nozzle angle increases. For a given nozzle angle, the thrust coefficient decreases as NPR increases. The thrust coefficients based on the CFD results are in general higher than the experimental and the discrepancy increases with increasing NPR. This discrepancy is likely due to the definition used to calculate the thrust coefficient from the CFD results, which neglects the base drag included in the experimental measurements. In Fig. 8(c), we plot the sonic lines at the throat of the three axisymmetric nozzles with the same pressure ratio of 2.5, and for each nozzle the agreement between the CFD, experimental, and theoretical is good. The sonic line is curved, and the curvature increases with increasing the nozzle angle. The sonic line is carried farther downstream for the higher nozzle angle. We also examined the effect of NPR on the sonic line location and found that the sonic line is moved to the throat with increasing pressure ratio, as seen in Fig. 8(d) for a 25° nozzle. The CFD result agrees well with the experimental data. However, for the case of NPR = 2.0, both computational and experimental data deviate from the theoretical data. Figures 9(a) and 9(b) compare the predicted shock structure to the experimental shadowgraphs for the axisymmetric nozzle and the nozzle bifurcated with the splitter plate, respectively. The predicted shock locations for both cases are in excellent agreement with the experimental results.

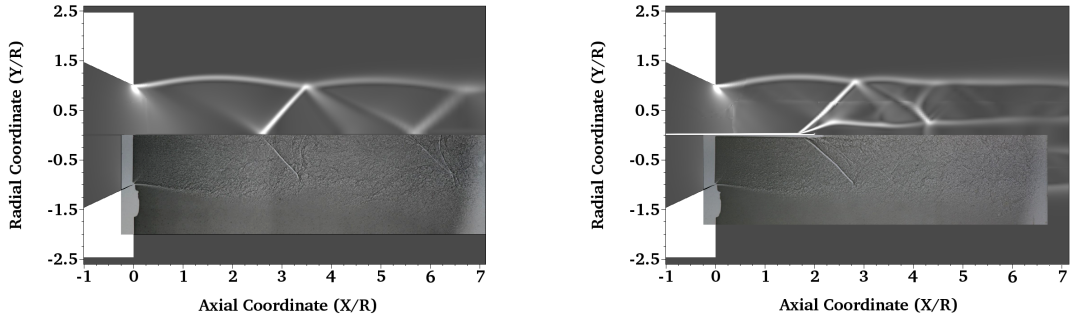

(a) Without splitter plate, top: CFD simulation and bottom: experimental data

(b) With splitter plate, top: CFD simulation and bottom: experimental data

Figure 9. The comparison between the numerical and experimental shock structures for the instance②.

IV. Concluding Remarks and Future Work

We performed a CFD study of the compressible flow through convergent-conical nozzles to investigate the effect of the nozzle pressure ratio and nozzle angle on the nozzle performance. We confirmed that the discharge coefficient increases as the nozzle angle decreases and the choked nozzle pressure ratio is lower for a smaller nozzle angle. The discharge coefficient increases with increasing pressure ratio until the choked condition is reached. The thrust coefficient increases as the nozzle angle increases, and for a given nozzle angle, the thrust coefficient decreases as nozzle pressure ratio increases. The results predicted by the CFD++ software generally are consistent with the literature data. However, our discharge coefficients are overpredicted, and this is likely due to the nonconservation of mass in the solutions. Future study includes a rigorous grid independence study and investigation of the algorithm techniques for enforcing conservation using an overset mesh.

V. Acknowledgments

The simulations were performed on the Colorado State University ISTeC HPC System supported by NSF Grant CNS-0923386. We thank the Metacomp Technologies, Inc. for their strong support of CFD++ software and many useful discussions.

References

[1]Thornock, R. L. and Brown, E. F., "An Experimental Study of Compressible Flow Through Convergent-Conical Nozzles, Including a Comparison With Theoretical Results," *Journal of Basic Engineering*, Vol. 94, No. 4, 1972, pp. 926–930.

[2]"Metacomp Technologies," http://www.metacomptech.com/.

[3]Zucrow, M. J. and Hoffman, J. D., *Gas Dynamics*, Wiley, 1976.

[4]Chang, L. and Chow, W., "Mach disk from underexpanded axisymmetric nozzle flow," *AIAA Journal*, Vol. 12, No. 8, 1974, pp. 1079–1082.